Supplementary Information (SI) for Soft Matter.
This journal is © The Royal Society of Chemistry 2025

Supplementary Information

Ultra-slow self-similar coarsening of physical fibrillar gels formed by semiflexible polymers

Martin Kröger,[a,b,*], Clarisse Luap,[c,*], and Patrick Ilg [d,*]

[a] *Computational Polymer Physics, Department of Materials, ETH Zurich, 8093 Zurich, Switzerland.*
[b] *Magnetism and Interface Physics, Department of Materials, ETH Zurich, 8093 Zurich, Switzerland.*
[c] *Independent researcher, 8049 Zurich, Switzerland.*
[d] *School of Mathematical, Physical, and Computational Sciences, University of Reading, Reading, RG6 6AX, United Kingdom.*

∗ *Corresponding author. E-mail: mk@mat.ethz.ch (M.K.), cluap@alumni.ethz.ch (C.L.), p.ilg@reading.ac.uk (P.I.).*

S1. Displacements

In Fig. S1 we choose a fixed value $t_w = 10^5$ of the waiting time and consider systems with $\kappa = 50$. This way characteristic jumps in the MSD corresponding to large-scale re-organizations of the network or breakage of fibers are well visible. Such jumps are smoothed out when averaging over realizations and/or time origins as in Fig. S1 and 15(c), respectively.

The three movies B-D (Tab. S-I) with $\delta t \in \{1,5,50\} \times 5000$ show 400 equidistantly spaced frames for the curve of realization no. 1 in Fig. S1, that extends over a time period of $t = 10^6$. Each movie uses its own coloring scheme which highlights bead displacement magnitudes between t and $t + \delta t$. The histogram of bead displacements is shown as well. This displacement histogram is proportional to $4\pi r^2 H_s(r,\delta t)$ with the self-part of the van Hove correlation function $H_s(r,\delta t) = \langle \delta(r - |\Delta \mathbf{r}(\delta t)|)\rangle$ and $\Delta\mathbf{r}(\delta t)$ the displacement of a given bead over a time interval δt. Normal diffusion corresponds to a Gaussian van Hove function with linearly increasing width, $H_s(r,\delta t) \to (4\pi D \delta t)^{-3/2} \exp(-r^2/4D\delta t)$ with D an assumed time-independent bead diffusion coefficient. For the network-forming systems investigated here, strong deviations from normal diffusion are reflected by i) a slower-than-linear growth of the spread of H_s with δt, ii) the slower-than square root growth of the mean displacement with δt, as well as iii) the large values of the non-Gaussian parameter α_2 seen in Fig. 15(d). The movies furthermore demonstrate that rare events of filament breakage and reorganization are associated with significant distortions of the displacement histograms. For example, pronounced jumps in $\langle \Delta r^2 \rangle(t)$ and $\langle \Delta r^4 \rangle(t)$ at about $t = 350000$ and $t = 995000$ are caused by filament breakage and/or significant rearrangement of one or more filaments. Varying δt allows us to visualize and quantify displacements over different time scales. Since the self-parts of the van Hove and intermediate scattering functions are related to each other via Fourier transformation, the movies visualize relaxation processes contributing to $F_s(q,\delta t)$.

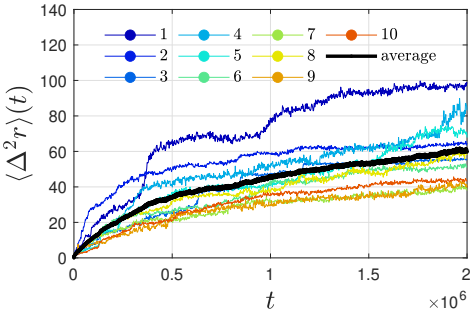

Fig. S1 **Unaveraged MSD**. (a,c) $\Delta(t,t_w) = \langle [\mathbf{r}(t+t_w) - \mathbf{r}(t_w)]^2 \rangle$ versus time t for all 10 independent realizations of the $N_c = 1000$, $\kappa = 50$ systems at a late stage of the coarsening $t_w = 10^5$. For realization no. 1 (uppermost curve) we provide supplementary movies A-D.

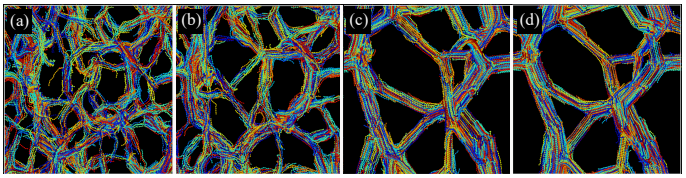

Fig. S2 **Ultra-slow coarsening**. Snapshots for the system with $N_c = 1000$ chains for $\kappa = 10$ at four different waiting times (a) $t_w = 0$, (b) $t_w = 1940$, (c) $t_w = 5 \times 10^4$, and (d) $t_w = 2.1 \times 10^6$. Note the marginal change between (c) and (d), where the network coarsens ultra-slowly.

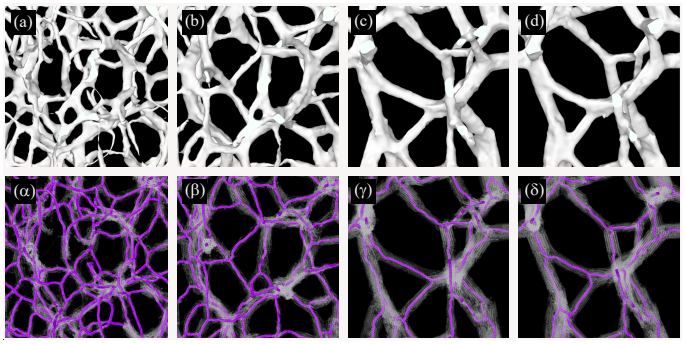

Fig. S3 **Morphometric analysis**. (a-d) Polymer surfaces and (α-δ) skeletons (purple lines) for the $\kappa = 10$ systems at the waiting times for which snapshots are shown in Fig. S2. In (α-δ) the polymer beads (semi-transparent) instead of the polymer surfaces have been rendered. Images were created with Ovito 3.10.6.

S2. Aging and ultra-slow coarsening

As detailed in the main text, the systems studied here show ultra-slow coarsening behavior, which leads to a waiting time dependence of various structural as well as thermodynamic quantities.

Snapshots, polymer surfaces and skeletons for the systems with

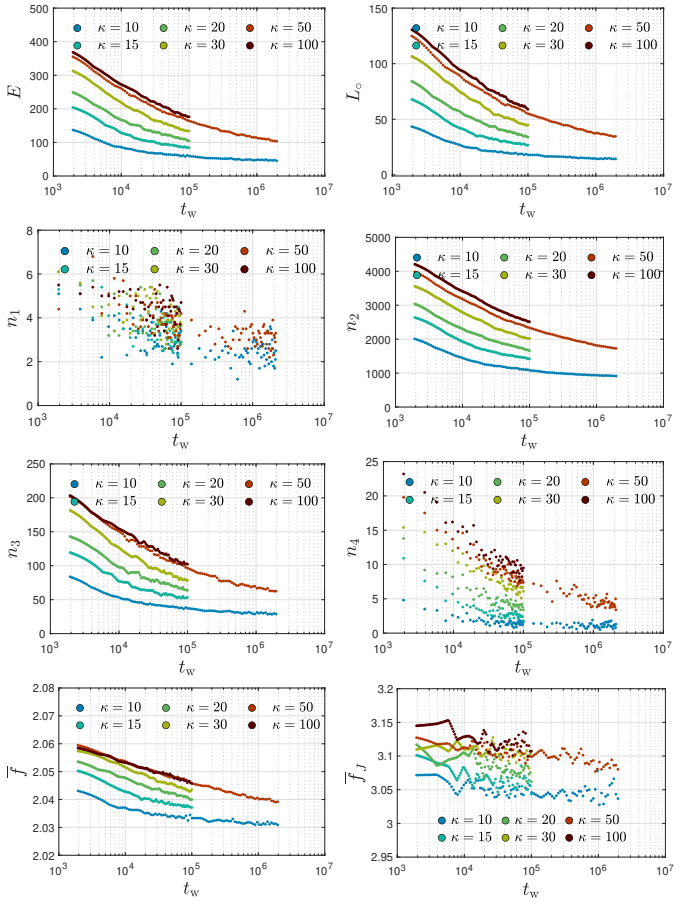

Fig. S4 **Skeleton analysis**. Time series averaged over 10 independent realizations. Number of edges E, number of loops $L_\circ$, number of f-functional skeleton beads n_f for $f \in \{1,2,3,4\}$ as defined in Sec. 5.4.2. In the last row: the mean functionality $\overline{f}$ of skeleton beads, and the mean junction functionality $\overline{f}_J$.

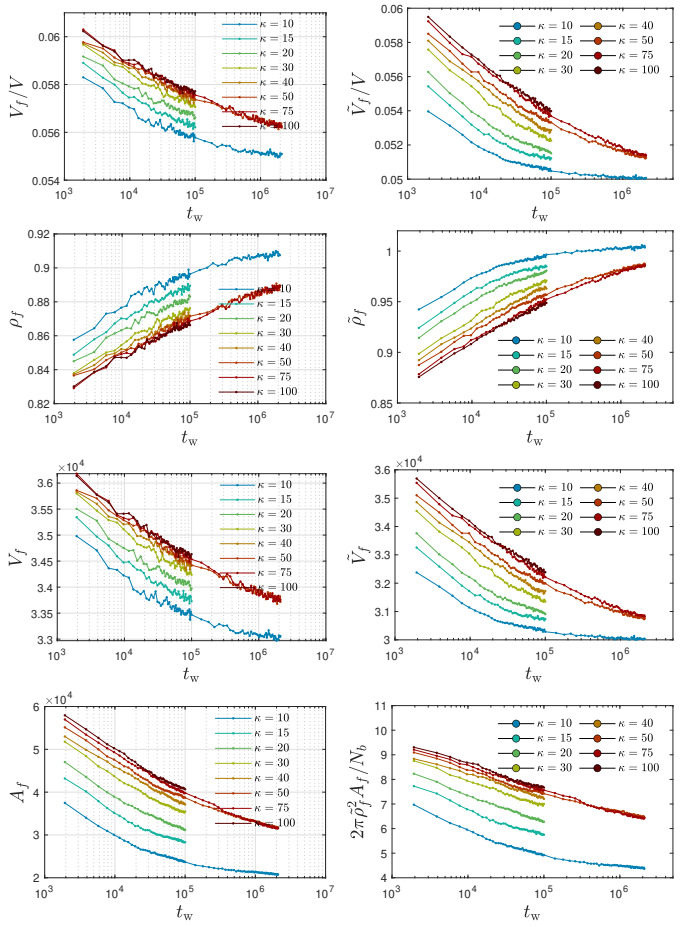

Fig. S5 **Morphometric analysis**. Total polymer surface area A_f and volume V_f of the filamentous network, number density $\rho_f = N_b/V_f$, and V_f/V versus waiting time t_w. While V_f and ρ_f were obtained from the accessible bead volume, $\tilde{\rho}_f$ and $\tilde{V}_f = N_b/\tilde{\rho}_f$ were calculated from the Voronoi volumes of skeleton beads (deep inside the filamentous bundles). Quantities were obtained using the methods described in Sec. 5.4.6.

$\kappa = 10$ at four different waiting times are displayed in Figs. S2 and S3. For all systems studied, time series for quantities characterizing the skeleton (skeleton bead functionalities n_f, number of edges and loops) are provided in Figure S4. Time series for surface area A_f, volume V_f of the filamentous network, $\tilde{V}_f$ obtained from voronoi volumes of skeleton beads, corresponding number densities ρ_f and $\tilde{\rho}_f$, mean weighted ℓ_0, ℓ_1, and unweighted chord lengths l_0, l_1 for the void and polymeric phases, obtained as described in section 5.4.6, are shown in Figs. S5–S6. Most of these quantities do not reach a stationary regime, and exhibit near-logarithmic growth, captured by Eq. (22).

Figure S7 shows the decrease of the total as well as the pair and bending energy per bead. As the system coarsens, potential energy contributions decrease, similar to aging amorphous materials. We show in Fig. S7 also network-specific quantities like the mean pore size, number of reversible bonds and polymer-specific quantities like gyration radius and persistence length. These figures further support our conclusions that pore sizes increase during coarsening, with chains straightening.

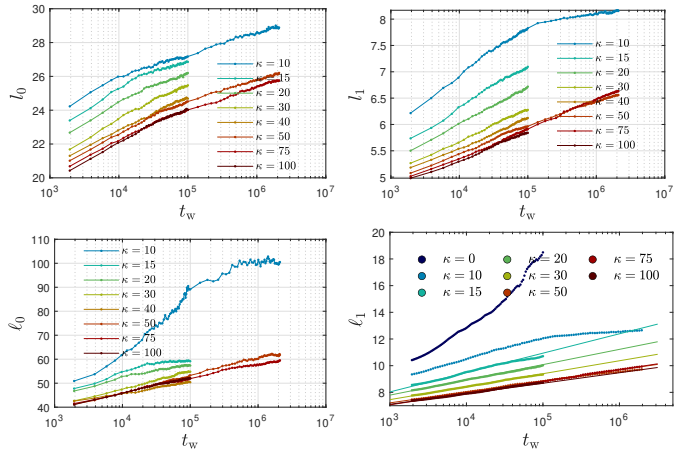

Fig. S6 **Mean chord lengths**. Time series, averaged over 10 independent realizations. Mean unweighted chord lengths l_0 and l_1, mean weighted chord lengths ℓ_0 and ℓ_1 versus waiting time t_w. Quantities were obtained using the methods described in Sec. 5.4.6. The lines in the l_1 panel are logarithmic fits (section Sec. S8).

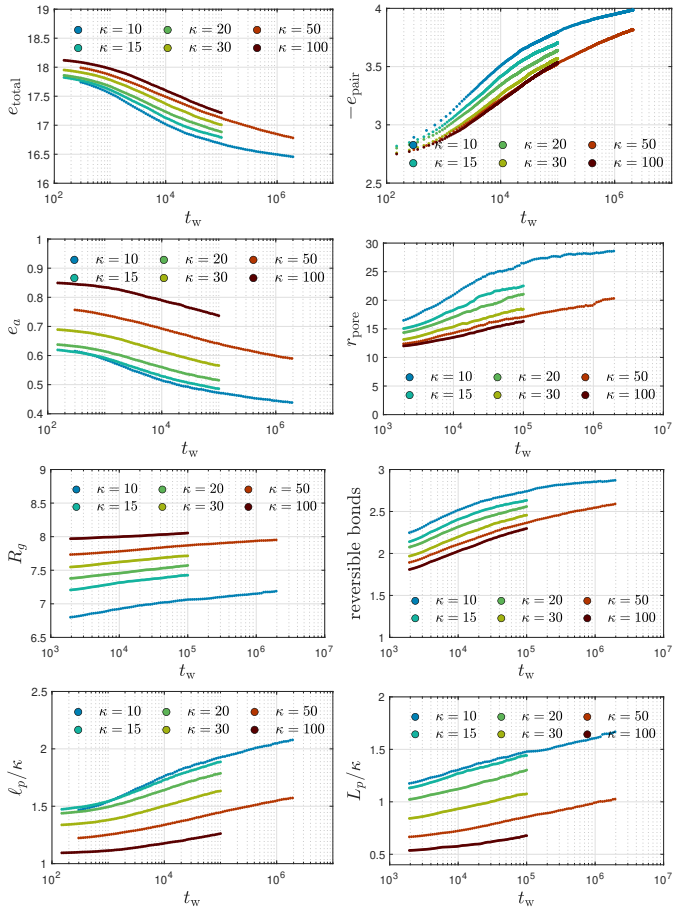

Fig. S7 **Energies, pore size, and gyration radius**. Time series, averaged over 10 independent realizations. Total energy per bead $e_{\rm total}$, pair contribution to total energy per bead $e_{\rm pair}$, bending energy per bead e_a, mean pore radius $r_{\rm pore}$, gyration radius R_g, number of reversible bonds per bead, reduced persistence length ℓ_p/κ obtained from e_a, and L_p/κ obtained from R_g.

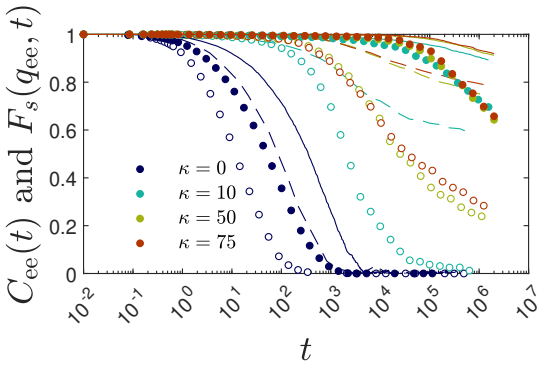

Fig. S8 **Orientational end-to-end vector dynamics**. Correlation functions $C_{\rm ee}(t)$ (lines) and $F_s(q_{\rm ee},t)$ (circles, for comparison) versus t for $t_{\rm w}=0$ (open circles, dashed lines) and $t_{\rm w}=10^5$ (filled circles, solid lines). For $\kappa=0$, 10, 50, and 75 the wave numbers are $q_{\rm ee}=2\pi/R=1.12$ (1.0), 0.32 (0.29), 0.26 (0.25), and 0.25 (0.24), respectively (numbers in brackets for $t_{\rm w}=10^5$), where R is the square root of the measured mean squared end-to-end distance at $t_{\rm w}$.

S3. Orientational relaxation of chains

Figure S8 shows the auto-correlation function $C_{\rm ee}(t)=\langle \mathbf{u}(t+t_{\rm w})\cdot \mathbf{u}(t_{\rm w})\rangle$ of the normalized end-to-end vector $\mathbf{u}=(\mathbf{r}_N-\mathbf{r}_1)/|\mathbf{r}_N-\mathbf{r}_1|$,

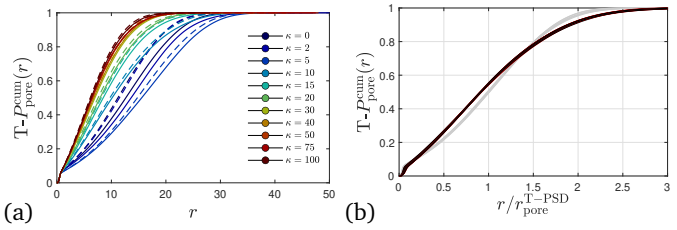

Fig. S9 **Self-similar pore size distribution**. (a) Cumulative pore size distribution T-$P^{\rm cum}_{\rm pore}(r)$ for comparison with the cumulative G-$P^{\rm cum}_{\rm pore}(r)$ shown in Fig. 9. For each κ we show data at $t_{\rm w}=5\times10^4$ (dashed) and $t_{\rm w}=10^5$ (solid). (b) Same data as shown in (a) but versus $r/r^{\rm T-PSD}_{\rm pore}$, where $r^{\rm T-PSD}_{\rm pore}$ is the time-dependent mean T-PSD pore radius. Solid and dashed curves fall onto two master curves at all times, onto the black solid line for all filamentous networks ($\kappa\geq10$), and onto the light gray curve for the droplet phase ($\kappa<10$). Panel (b) remains unchanged if we include data at larger $t_{\rm w}$.

averaged over all N_c chains and 10 independent realizations of the system. Two different waiting times are considered, $t_{\rm w}=0$ and $t_{\rm w}=10^5$. In the network-forming regime for semiflexible chains with $\kappa\geq10$, relaxation of the end-to-end vector barely proceeds on the time scales of the simulations (see Fig. S8) but we still observe the relaxation times to increase with increasing $t_{\rm w}$. For the percolated networks, loss of orientational memory can only be achieved for dangling ends (including ruptured filaments). Only in the droplet phase with rather flexible chains does the correlation function $C_{\rm ee}(t)$ decay to zero, i.e. achieves full relaxation, as the individual droplets can rotate freely. These observations are in qualitative agreement with those made for the self part of the intermediate scattering function $F_s(q,t)$ (Fig. 17).

In analogy to the self-intermediate scattering function $F_s(q,t)$, the end-to-end vector relaxation can be characterized in terms of an effective relaxation time $\tau_{\rm ee}$ defined by $C_{\rm ee}(\tau_{\rm ee})=0.5$. To compare $\tau_{\rm ee}$ to $\tilde{\tau}_q$ derived in this way from $F_s(q,t)$ (see Fig. 19), we estimate a corresponding scattering vector $q_{\rm ee}$ from random walk statistics, $R\approx\langle R^2\rangle^{1/2}_{\rm RW}$ with $\langle R^2\rangle_{\rm RW}=b^2(N-1)$ via $q_{\rm ee}=2\pi/R$. For $\kappa=0$ one therefore has $q_{\rm ee}\approx1.2$ so that $R_{\kappa=0}\approx5.3$. More accurate values of R are available from R_g and L_p. From Fig. 17, we can read off a characteristic relaxation time $F_s(1,\tilde{\tau}^{\kappa=0}_{q=1})=0.5$ of $\tilde{\tau}^{\kappa=0}_{q=1}\approx20$ and 40 for $t_{\rm w}=0$ and 10^5, respectively, while the corresponding $\tau_{\rm ee}$ for $\kappa=0$ is about a factor of five larger. Comparing in the same way $\tilde{\tau}_{q_{\rm ee}}$ and $\tau_{\rm ee}$ for other values of κ, one needs to take into account that R increases and therefore $q_{\rm ee}$ decreases with increasing κ. Figure S8 shows a comparison of $C_{\rm ee}(t)$ and $F_s(q_{\rm ee},t)$ where the corresponding wave numbers $q_{\rm ee}$ are calculated from the simulation data of the end-to-end distances at the given values of κ. Their values are given in the figure caption. From Fig. S8 we find that orientational relaxation proceeds significantly slower compared to structural relaxation on the same length scale. Therefore, we conclude that structural relaxation on the length scale of the end-to-end vector is governed by cooperative rearrangements, while single chain orientational relaxation play a minor role, especially for the percolated systems.

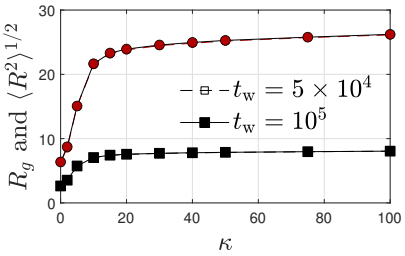

Fig. S10 **Chain dimensions**. Square root of the mean squared end-to-end distance (red circles) and radius of gyration (black squares), at two different times (the symbols overlap). Their ratio, varying between $\sqrt{6}$ (random coils) and $\sqrt{12}$ (rods) is used to estimate the "global" persistence length (Sec. 5.2).

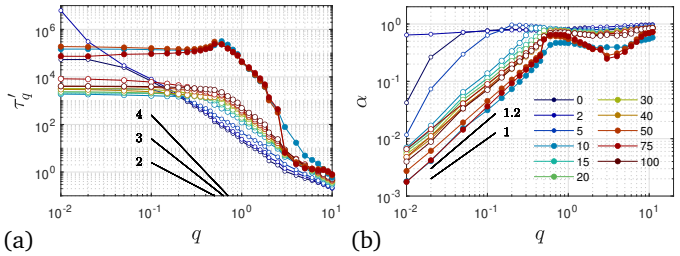

Fig. S11 **Power-Mittag-Leffler parameters**. (a) Characteristic time τ'_q of the power-ML function (6) versus the wave number q extracted from the incoherent scattering function, for several κ (legend). Panel (b) shows the data of Fig. 18 in a double-logarithmic representation. Open circles correspond to $t_w = 0$ (all κ), while filled circles are for $t_w = 10^5$ ($\kappa \in \{10,50,75\}$ only).

S4. Torquato's pore size distribution (T-PSD)

The cumulative pore size distribution T-$P^{\rm cum}_{\rm pore}(r)$ for comparison with the cumulative G-$P^{\rm cum}_{\rm pore}(r)$ (Fig. 9) is shown in Fig. S9(a). As one may expect from the existence of a master curve for the distribution of weighted chord lengths for the filamentous networks, the T-$P_{\rm pore}(r)$ falls onto a master curve as well, shown by the solid black line in Fig. S9(b), where we plot T-$P^{\rm cum}_{\rm pore}(r)$ versus $r/r^{\rm T\text{-}PSD}_{\rm pore}$. The droplet systems with $\kappa < 10$ give rise to a second, slightly different master curve (light gray).

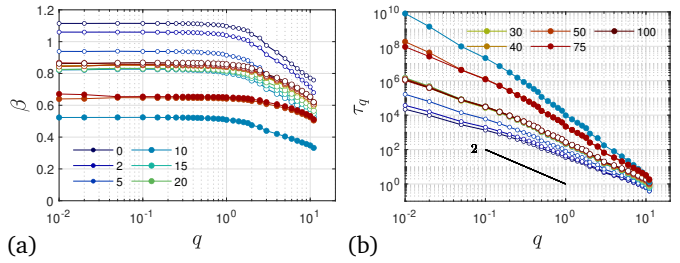

Fig. S12 **Stretched exponential parameters**. (a) Exponent β and (b) relaxation time τ_q characterizing the stretched exponential behavior at very short times, $t < 1$. Open circles correspond to $t_w = 0$ (all κ), while filled circles are for $t_w = 10^5$ ($\kappa \in \{10,50,75\}$ only). Legend in (a) valid for (b) as well.

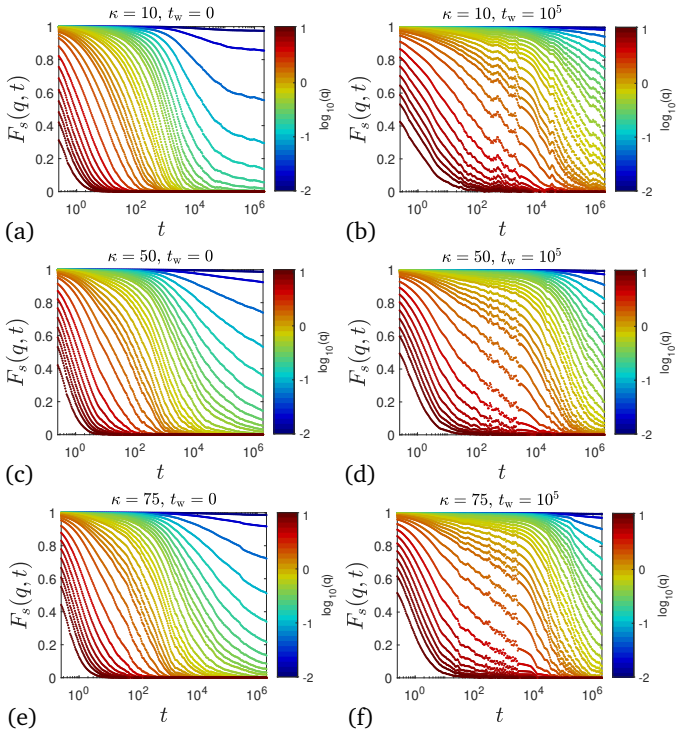

Fig. S13 **Incoherent scattering function**. Measured self part of the intermediate scattering function $F_s(q,t)$ versus t, averaged over 10 independent realizations, for (a) $\kappa = 10$ at $t_w = 0$, (b) $\kappa = 10$ at $t_w = 10^5$, (c) $\kappa = 50$ at $t_w = 0$, (d) $\kappa = 50$ at $t_w = 10^5$, (e) $\kappa = 75$ at $t_w = 0$, and (f) $\kappa = 75$ at $t_w = 10^5$. The value of q is specified by the logarithmic color bar.

S5. Incoherent scattering function

To fit the measured data for $F_s(q,t)$ we used the three-parametric $\tilde{F}_s(q,t)$ defined in Eq. (6). The two exponents α and β are shown in semilogarithmic Fig. (18). The remaining fitting parameter τ'_q is displayed in Fig. S11(a). As mentioned in Sec. 5.3 already, at large $t \gg \tau'_q$, the $\tilde{F}_s(q,t)$ approaches a power-law regime, $\tilde{F}_s(q,t) = (t/\tau''_q)^{-\alpha}$ with $\tau''_q/\tau'_q = [1/\Gamma(1-\beta)]^{1/\beta}$. Figure S11(b) shows α in a double-logarithmic plot, highlighting a regime $\alpha \sim q^{6/5}$ at low q. The three-parametric fit function has the feature, that it does not guarantee the measured short and long time asymptotic behaviors (both characterized by two variables) to be reproduced perfectly. Such a constraint would require an additional fitting parameter. The β values obtained from a fit of the short time $t < 1$ behavior of $F_s(q,t)$ to a stretched exponential are shown in Fig. S12. Except for droplet phases with $\kappa \le 2$, the so-obtained β's do not exceed unity and as expected, these β values do not fully agree with the fitting parameter β of the power-ML (Fig. S11-b). They approach constant values in the limit $q \to 0$. We verified that the fits of $F_s(q,t)$ do not improve significantly upon adding a fourth parameter γ in expressions such as $\{E_\gamma[-(t/\tau'_q)^\beta]^{\alpha/\beta}\}$.

S6. Additional snapshots

Additional snapshots at waiting time $t_w = 10^5$ for selected realizations of systems with $N_c = 1000$ chains at $\kappa = 5$ and $\kappa = 10$ are shown in Fig. S14. We find that both systems can exhibit two qualitatively different types of structures. For $\kappa = 5$, the num-

Movie	κ	realization	t_w	duration	filename	content
A	50	1	1.28×10^6	1.5×10^5	kappa=50-tw=1e5-copy=1-rupture.gif	filament rupture event
B	50	1	10^5	2×10^6	kappa=50-tw=1e5-copy=1-dframes=1.mp4	displacements, $\delta t=5\times10^3$
C	50	1	10^5	2×10^6	kappa=50-tw=1e5-copy=1-dframes=5.mp4	displacements, $\delta t=2.5\times10^4$
D	50	1	10^5	2×10^6	kappa=50-tw=1e5-copy=1-dframes=50.mp4	displacements, $\delta t=2.5\times10^5$
E	5	11	-10^3	2×10^3	kappa=5-init-chain-color-openr.mp4	droplet formation
F	10	11	-10^3	2×10^3	kappa=10-init-chain-color-openr.mp4	network formation
G	50	11	-10^3	2×10^3	kappa=50-init-chain-color-openr.mp4	network formation
E+	5	11	10^3	2×10^4	kappa=5-tw=1e3-chain-color.mp4	coarsening dynamics
F+	10	11	10^3	2×10^4	kappa=10-tw=1e3-chain-color.mp4	coarsening dynamics
G+	50	11	10^3	2×10^4	kappa=50-tw=1e3-chain-color.mp4	coarsening dynamics
H	5	1	0	10^5	kappa=5-tw=0-copy=1-chain-color-B.mp4	droplets and short cylinders
I	5	6	0	5×10^4	kappa=5-tw=0-copy=6-chain-color.mp4	percolated cylinder
J	20	1	0	5×10^4	kappa=20-tw=0-copy-1-chain-color.mp4	coarsening dynamics

Table S-I Summary of collected movies for systems with 1000 chains ($N=30$) at number density $\rho=0.05$. All movies available from our Github repository https://github.com/mkmat/FENE-CB-model. Alternatively, you can click on the filename in the above table.

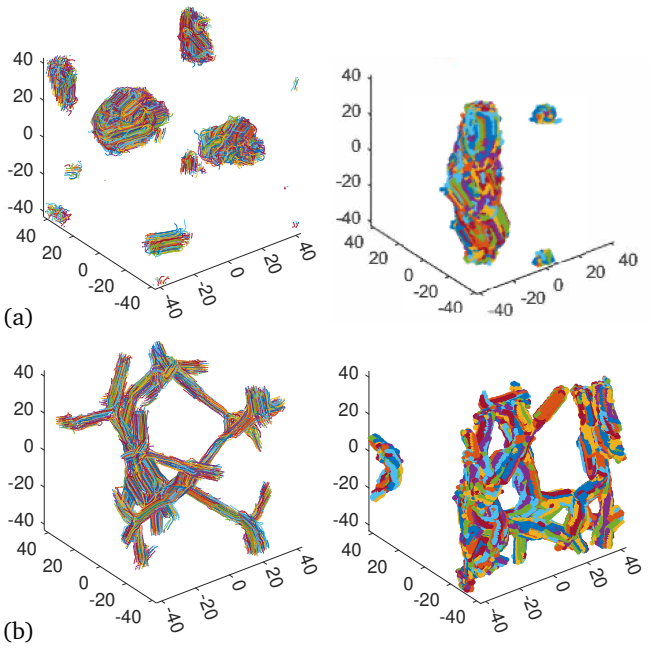

Fig. S14 **Selected snapshots** for four independent realizations of systems with (a) $\kappa=5$ and (b) $\kappa=10$ at waiting time $t_w=10^5$ since system preparation. Each chain has its own color. For $\kappa=5$ and $\kappa=10$ two qualitatively different configurations are shown (unpercolated and percolated in one dimension for $\kappa=5$, and percolated in 3 and 2 dimensions for $\kappa=10$). For both κ, the second scenario occurred in only 2 out of 10 realizations.

ber of near-spherical and near-cylindrical droplets varies, and in 2 out of 10 realizations the system is percolated in one direction through the formation of a single near-cylindrical strand that is connected to itself via the periodic boundaries. For $\kappa=10$, in 2 out of 10 realizations we observed the formation of a network that is percolated over two dimensions only. Both, the formation of a single strand and the two-dimensional network can be considered as finite size effects, as the probability for their formation decreases with increasing system size. In fact, we did not observe them for the larger systems with $N_c=50000$ chains at unchanged κ.

S7. Movies

We offer several types of movies (Tab. S-I) showing animated sequences of selected systems. All movies were made using Ovito 3.10.6.

(i) **Movie A** displays a selected filament rupture event for the aged $\kappa=50$ system ($t_w=10^5$, realization 1). This rupture event is associated with the first large jump in the MSD of Figs. S1 and 16. Beads are colored according to their displacement magnitude.

(ii) **Movies B,C,D** show the time evolution of an aged system between $t_w=10^5$ and $t_w=2.1\times10^6$ (400 frames, frame rate 1/5000) for $\kappa=50$ along with the animated bead displacement histogram. The first frame, labeled by $t=0$, corresponds to $t_w=10^5$. In each frame at time t_w+t, displacement vectors are colored by their actual displacement magnitude $|\mathbf{r}_j(t_w+t+\delta t)-\mathbf{r}(t_w+t)|$, where $\delta t/5000=1,5,50$ for movies B,C,D, respectively. The first and last beads of each chain are rendered in red and yellow. A snapshot of movie C is shown in Fig. S15. The movies highlight those strands that break or dislocate. The different spacings δt allow to estimate the lag time required for large displacements to occur, and they correspond to the choice of different δt values in the calculation of the self-intermediate scattering function $F_s(q,\delta t)$, as mentioned in Sec. S1 already.

(iii) **Movies E,F,G** show the formation of the systems for $\kappa=5$, 10, and 50, respectively, all starting at $t_w=-1000$. Frame rate 1/5. Movies E+,F+,G+ show the continuations of movies E,F,G, starting at $t_w=1000$ at frame rate 1/50.

(iv) **Movie H** (screenshot in Fig. S16) shows the formation of droplets and near-cylindrical bundles for one of the $\kappa=5$ realizations starting at $t_w=0$ for a duration of 10^5 (400 frames, frame rate 1/250). Here, each chain has its own color. The last frame of movie H is displayed in Fig. S14-a. **Movie I** (screenshot in Fig. S16-b) shows the formation of a percolated cylinder, again for $\kappa=5$.

(v) **Movie J** provides a visualization of the $\kappa=20$ system between $t_w=0$ and $t_w=5\times10^4$.

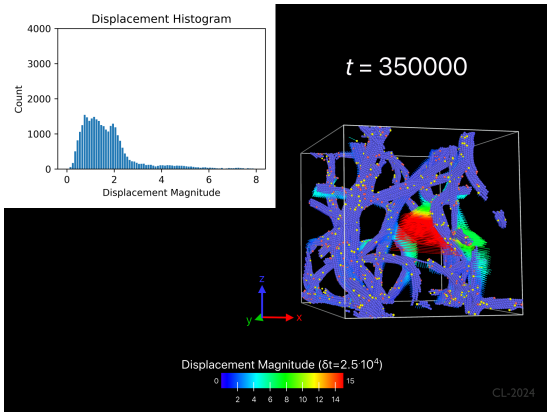

Fig. S15 **Screenshot** of movie C ($\kappa = 50$, realization no. 1, $t_w = 10^5$) highlighting the large displacement magnitudes produced by a filament rupture event occurring between $t = 350000$ and $t = 375000$ ($\delta t = 25000$). The inset shows the histogram of displacement magnitudes (bin size 0.1). According to Eq. (14), for a given t, δt and q, the fraction of beads with a displacement magnitude Δr below q^{-1} essentially determines the value of $F_s(q, \delta t)$, that one would measure at an aging time $t_w + t$.

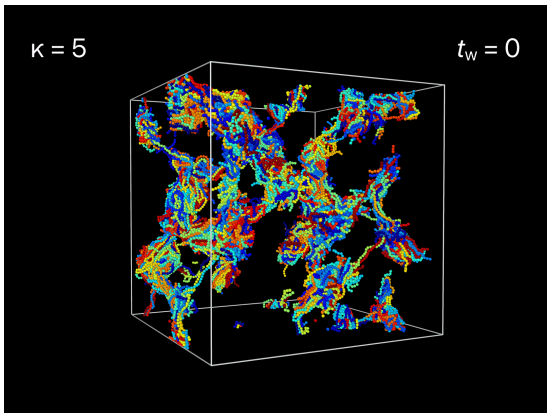

Fig. S16 **Screenshot** of the first frame of movie H at $t_w = 0$.

S8. Github repository

The logarithmic fits described in Sec. 5.5.2 have been created for various measured timeseries, including L_f, d_f, n_f, V_f, l_0, l_1, R_g etc. Instead of collecting the four fitting parameters for each quantity here, we provide a script that allows to evaluate and visualize the fitted curves. The script is available at our Github repository `https://github.com/mkmat/FENE-CB-model`. This repository furthermore provides links to all movies, and a LAMMPS script that allows to redo the simulations.